Automatic Extraction of Signal Areas from Radio Spectrograms Based on the Hough Transform

Mohammed M. Alammar*†, Miguel López-Benítez*‡ and Janne Lehtomäki§
*Department of Electrical Engineering and Electronics, University of Liverpool, United Kingdom
†Department of Electrical Engineering, King Khalid University, Abha, Saudi Arabia
‡ARIES Research Centre, Antonio de Nebrija University, Madrid, Spain
§Centre for Wireless Communications, Department of Communications Engineering, University of Oulu, Finland
Email: m.m.alammar@liverpool.ac.uk, m.lopez-benitez@liverpool.ac.uk, janne.lehtomaki@oulu.fi

***Abstract*—Radio communication signals are often represented in many practical application scenarios as a spectrogram, which indicates the power observed at several discrete time instants and frequency points within a certain time interval and frequency band, respectively. The concept of Signal Area (SA) was recently introduced in the context of spectrum occupancy measurements as the rectangular region in the time-frequency domain where a signal is believed to be present. An accurate estimation of the original SA for each radio transmission contained in a spectrogram can provide valuable information in many practical application scenarios, such as autonomous spectrum-aware wireless communication systems. In this context, this work proposes new methods for an accurate Signal Area Estimation (SAE) based on the application of the Hough Transform (HT) combined with other techniques from the field of image processing. The performance of the proposed methods is evaluated by means of simulations and experiments. The obtained results show that they can achieve a high level of SAE accuracy. Moreover, an interesting and distinguishing feature of the proposed methods is their ability to not only improve the accuracy of the SAE but also to extract automatically the coordinates and dimensions of each SA detected in a radio spectrogram. This feature can be useful in the automatic processing of radio spectrograms, for example in the context of autonomous spectrum-aware wireless systems.**

***Index Terms*—Wireless communications, spectrum measurements, signal area, Hough transform, image processing.**

I. Introduction

The occupancy in the joint time-frequency domains of a spectrum band used for radio communications can be conveniently represented by means of spectrograms. Radio spectrograms provide information about the power spectral density of a signal (or a set of signals) that are present in the frequency band of interest at regular time intervals. Spectrograms can be processed to extract relevant information about the signals presents in a certain band, such as for example the received signal strength, carrier frequency, occupied bandwidth, spectral mask and transmission pattern. Among the many signal parameters that can be extracted from a spectrogram, the interest of this work is on determining the time-frequency region of the spectrogram that is occupied by each radio transmission or signal component present in the spectrogram, which has been referred to in the literature as Signal Area (SA) [1]. A SA is a group of spectrogram points or elements arranged in a rectangular cluster where a certain signal is believed to be present. Each of such points or elements of the spectrogram corresponds to a measured time slot and frequency bin in the time and frequency domains, respectively. The dimensions of each SA within a spectrogram indicate the bandwidth occupied by each radio transmission as well as its start and end times. The ability to obtain this information from a spectrogram can be of significant utility in a broad range of practical scenarios that include spectrum surveillance for enforcement of spectrum regulations, gathering of signal intelligence in military environments, signal interception and identification, and spectral awareness for dynamic spectrum sharing applications [1]–[3], among many others.

A number of Signal Area Estimation (SAE) methods have been proposed in the literature based on different operating principles [1], [4]–[15]. Some popular methods include fast Fourier transform-based energy detection (ED-FFT) [14], Contour-Tracing (CT-SA) algorithms [11], and the so-called Simple Signal Area (SSA) algorithm proposed in [1], [12], [13]. In this context, this work considers a different approach based on the application of image processing techniques to radio spectrograms. The use of image processing methods to the problem of SAE is motivated by the fact that the problem of estimating a SA in a noisy spectrogram is similar to the problem or recognising a rectangle in a noisy image. By interpreting each radio spectrogram point (indicating a binary occupied/empty state) as a pixel in a binary (black-and-white) image, spectrograms can be seen as images, which enables the application of several powerful image processing techniques to the problem of SAE, concretely, the estimation of solid rectangular shapes degraded by the presence of noise and radio propagation impairments.

Several image processing techniques can be used to identify shapes after separating them from their background (noise) [16]. One such technique that is particularly suited to the problem of SAE considered in this work is the Hough transform (HT). The HT can be employed to recognise lines and rectangular shapes and is therefore an appropriate tool to identify SAs in a radio spectrogram. This paper explores the usability of the HT in the context of SAE and proposes two approaches that exploit the HT to estimate SAs in a spectrogram. The main interest of the proposed methods, and a distinguishing feature with respect to most other methods proposed in the literature, is their ability to automatically extract

the parameters of each SA (i.e., the coordinates of the vertical and horizontal lines containing each SA). Most of previously proposed SAE methods produce enhanced spectrograms where the present SAs can be appreciated more accurately, however have not typically been designed to automatically provide the coordinates and dimensions of each SA. On the other hand, the HT-based methods proposed in this paper can provide not only an enhanced spectrogram but also the coordinates and dimensions for each of the SAs detected in such spectrogram. This feature can be extremely useful in the automatic processing of radio spectrograms, for instance in the context of autonomous spectrum-aware wireless and mobile communication systems.

The rest of the paper is organised as follows. First, Section II provides a formal description of the SAE problem considered in this work along with an overview of SAE techniques proposed in the existing literature. Section III provides an overview of the basic principles of the HT and presents the two new methods proposed in this paper. Section IV then describes the methodology employed in this work to assess the estimation accuracy of the proposed methods. The obtained results are then presented and analysed in Section V. Finally, Section VI summarises and concludes the study.

II. Signal Area Estimation

A. Problem Description and Formulation

SAE methods are applied to spectrum readings based on two-dimensional time-frequency grids of spectrum data. The time-frequency grids consist of clustered tiles where each element reflects the signal presence state in the corresponding time and frequency point. In power spectrograms, each tile represents a continuous-domain power value, which can be mapped to a discrete-domain occupied/empty state by using an appropriate decision threshold [17]. The appropriate configuration of such decision threshold in the context of SAE has been investigated in [18]. This binary time-frequency grid provides the fundamental data required for SAE and is the input information that most SAE methods need, based on which they will attempt to estimate as accurately as possible rectangularly-shaped regions containing adjacent tiles in the occupied state. Each of such regions is referred to as a Signal Area (SA) and it univocally identifies the occupied bandwidth and duration of each radio transmission. Notice that, by definition, most wireless communication signals should produce a rectangularly-shaped SA – or a set of rectangular SAs in the case of certain particular signal formats (e.g., frequency hopping signals). However, due to the degradation introduced by the presence of noise and the radio propagation channel, the SAs present in the spectrogram observed at the radio receiver will not necessarily have a perfectly rectangular solid shape. The purpose of SAE methods is to attempt to reconstruct the original rectangular SAs produced by the transmitter activity based on the imperfect/degraded version observed at the receiver.

The detection and estimation of SAs in a real radio spectrogram is accompanied by a set of limitations that resemble those of the classical signal detection process [19]. The accuracy of SAE depends on the occurrence of the same types of signal detection errors, namely missed detections and false alarms, which are common errors in signal detection procedures where busy and idle tiles may be detected in their opposite states. Missed detections and false alarms compromise the shape of the observed SAs and interfere with the operation of SAE methods. However, it is worth noting that the ultimate purpose of SAE methods is different from that of signal detection techniques. Signal detection techniques are aimed at accurately detecting the instantaneous presence of a signal in a certain frequency band and therefore it is important to produce an accurate detection in every time-frequency tile. However, on the other hand, SAE is concerned with an accurate estimation of the overall SA but certainly pays minimal attention to the accuracy of individual tiles as long as the overall SA can be estimated accurately. This is because the aim of SAE methods is to establish the time-frequency region occupied by each SA rather than the customary instantaneous signal presence in each time-frequency point of the spectrum. Moreover, signal detection methods are usually aimed at providing real-time decisions on the instantaneous (current) spectrum occupancy state, while SAE methods are usually not envisaged to be applied in real-time (which would certainly be not possible due to the time span needed to capture the amount of data required to complete a spectrogram). SAE methods are typically employed for offline processing of spectrum occupancy data and its characterisation in the longer-term.

B. Existing SAE Methods

A number of methods have been proposed in the literature to estimate accurately the SAs present in a radio spectrogram based on the (degraded) signal power data observed at the receiver [1], [4]–[15]. Some popular methods include fast Fourier transform-based energy detection (ED-FFT) [14], Contour-Tracing (CT-SA) algorithms [11], and the so-called Simple Signal Area (SSA) algorithm proposed in [1], [12], [13]. A popular approach that has been usually employed is ED-FFT [14] given its simplicity and low computational cost. This approach simply determines the busy or idle state of every point/tile in the time-frequency domain using a tile-by-tile ED-FFT [20]. ED-FFT methods are simple and convenient but do not necessarily produce a rectangular estimation for each SA, thus they tend to be more inaccurate. In any case, ED-FFT can be used as a useful baseline for reference to compare with other SAE methods including the new methods proposed in this work. A more evolved approach is CT-SA, where a rectangular SA is approximated by using contour tracing techniques [11]. A more powerful and accurate SAE method is the SSA algorithm proposed in [1], [12], [13], which is a sophisticated method of estimating the SA in the time-frequency domain in a series of steps. The steps in SSA include raster scan to detect the first corner of a potential SA, horizontal scan to evaluate the width of the SA, a coarse estimation of the SA height and finally a fine height estimation procedure to determine the approximate total dimensions of the SA. More recently, a *Minesweeper* Algorithm (MA) has

been proposed in [15], which decides the state of each tile based on its own state and the states of neighbouring tiles. The MA method is heuristic and does not necessarily produce a rectangular SA either but it has been proven to provide significant accuracy improvements when combined with the CT-SA and SSA methods as a pre/post-processing technique.

III. Signal Area Estimation based on the Hough Transform

A. Motivation

The problem of SAE in a time-frequency grid of discrete occupied/empty elements (obtained by appropriately thresholding a spectrogram of continuous-power values) is similar to the problem or recognising a rectangular shape in a noisy binary image. By interpreting each radio spectrogram point (indicating a binary occupied/empty state) as a pixel in a binary (black-and-white) image, spectrograms can be seen as images, which enables the application of several powerful image processing techniques to the problem of SAE, concretely, the estimation of solid rectangular shapes degraded by the presence of noise and radio propagation impairments. This point of view motivates the exploration of powerful tools from the field of Image Processing in the context of SAE. Image Processing is a well-developed field that counts with advanced and sophisticated techniques to detect shapes in noisy images. One such technique that is particularly suited to the problem of SAE considered in this work is the Hough transform (HT). The HT can be employed to recognise lines and rectangular shapes and is therefore an appropriate tool to identify SAs in a radio spectrogram [21]. This paper explores the usability of the HT in the context of SAE and proposes two approaches that exploit the HT to estimate SAs in a spectrogram.

B. Overview of the Hough Transform

The HT is a feature extraction technique whose purpose is to identify imperfect instances of objects in an image. The HT originated from the basic need to detect certain shapes inside arbitrary images corrupted by noise and other artefacts. In its most basic definition, the classical HT was concerned with the identification of lines in an image, while the generalised HT was later on introduced to enable the detection of more complex arbitrary shapes such as circles or ellipses and their positions within images. Notice that SAs are by definition rectangularly shaped and therefore are delimited by four lines corresponding to the edges of the SA. Such straight lines can be detected with a classical HT and therefore the interest of this work lies on the classical HT [22], [23].

The HT detects imperfect instances of a certain shape (in the case concerned in this work, straight lines) based on a voting procedure carried out over parametised image objects. Basically, each possible candidate shape (line) is represented according to a given parameter space and then all possible candidates are tested by assessing how closely they match with the pixels of the image. The best fitting candidate is then selected by means of a voting procedure. Lines are typically represented in a Cartesian x-y space in the form $y = mx + n$,

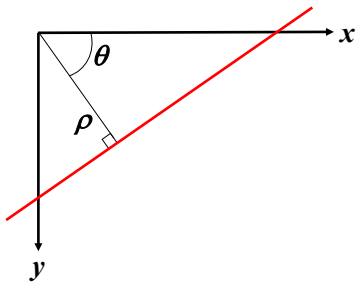

Fig. 1: Parameter space for the Hough transform.

where m is the slope of the line and n its displacement with respect to the origin. Thus, in a Cartesian space each line can be represented as a point (m, n) in the parameter space. This parameter space, however, has the inconvenience that vertical lines would give rise to unbounded values of the slope parameter ($m \to \infty$), which would pose computational problems. For this reason, the HT is carried out over a Hessian normal form $\rho = x\cos\theta + y\sin\theta$, where ρ is the distance from the origin to the closest point on the straight line and θ is the angle between the abscissas axis and the line connecting the origin with that closest point, as illustrated in Fig. 1. In this parameter space, each line is represented as a point (ρ, θ). The result of the HT is a matrix whose elements are used as accumulators indicating the frequency of occurrence of the potential lines observed for each pair (ρ, θ). In the context of SAE, the SAs can be assumed to be aligned with the x-y axes of the Cartesian space and therefore each SA can be assumed to be delimited by two pairs of mutually parallel lines, a pair of vertical lines ($\theta = 0$) and another pair of horizontal lines ($\theta = \pi/2$). The abscissas (x) coordinates of vertical lines are then obtained as the value of ρ in the HT for $\theta = 0$, while the ordinates (y) coordinates of horizontal lines are obtained as the value of ρ in the HT for $\theta = \pi/2$ as illustrated in Figs. 2 and 3. As a result, the HT can automatically provide the coordinates of the lines that correspond to the edges of each SA. Having the coordinates of the lines that delimit the SAs in a radio spectrogram, it is possible to extract the coordinates and dimensions for each individual SA in a radio spectrogram. This is a significant advantage of HT-based SAE compared to most existing SAE methods, many of which have not been specifically designed to obtain this information (despite of its importance in practical applications) in an automated manner (i.e., without human manual intervention).

C. Proposed HT-based SAE methods

The proposed SAE methods, similar to many other SAE methods, are based on the processing of binary spectrograms where each spectrogram point contains a binary value indicating whether a signal component is believed to be present or not. Such spectrogram can be obtained by thresholding a continuous-domain power spectrogram. The configuration of such threshold as well as the resolution of the spectrogram can have a significant impact on the performance of SAE methods.

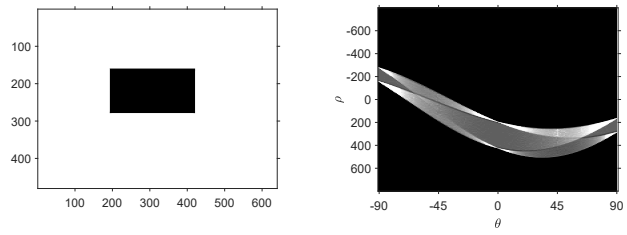

(a) (b)

Fig. 2: HT example with 1 SA: (a) spectrogram, (b) HT.

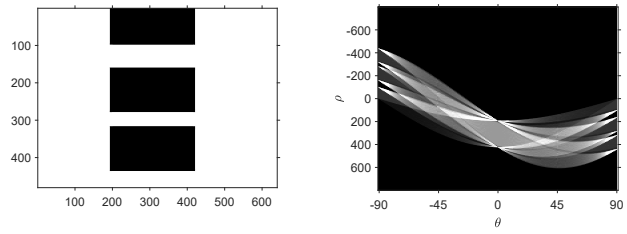

(a) (b)

Fig. 3: HT example with 3 SAs: (a) spectrogram, (b) HT.

These aspects are out of the scope of this work but a detailed analysis and discussion can be found in [18].

The examples shown in Figs. 2 and 3 correspond to ideal cases where a perfect SA is observed without any degradation. In a real radio spectrogram obtained from actual empirical measurements there will be artefacts in the image in the form of false alarms (introduced by the noise present at the radio receiver) and missed detections (caused by radio propagation impairments). Missed detections will in general not be a source of major concerns since they will often occur inside SAs and therefore will be surrounded by other points in occupied/busy state that will help detect the SA. However, false alarms can lead to significant detection performance degradation (the same effect was also observed and discussed in [1] in the context of SAE). False alarms are particularly problematic in the application of the HT because each false alarm point will be processed by the HT algorithm by trying to identify lines that pass through that point. A large number of false alarms may therefore have a significant impact on the HT output. To address this problem, a false alarm reduction step is first applied by convolving the input binary image with a 3×3 filter whose template is composed of all ones. The busy points with an output value lower than or equal to two (i.e., isolated points not surrounded by a significant number of other busy points) are deemed to be false alarms rather than true SA points and therefore discarded (their value is inverted to the free/empty state). This process is similar to that employed by the MA method described in [15].

After the input spectrogram has been filtered to reduce the incidence of false alarms, the resulting cleaner image can be more accurately processed with a HT. However, the HT is rarely directly applied to an image. It is often a common practice to first apply an edge detection method in order to extract the edges of those objects present in the image. In the case of a radio spectrogram, this edge detection step will highlight and show more clearly the potential lines (edges of the SAs) present in the image. In this work, the Canny edge detector [24] is selected due to its ability to account for image noise [25] and its higher detection performance compared to other conventional edge detectors. Notice that an edge detector will provide a more clear visualisation of the lines delimiting the SAs in a spectrogram, however such edges will be imperfect in the sense that they will usually not be a clear and well-defined single straing line at a unique coordinate. Instead, due to the presence of noise and radio propagation degradation, each side of a SA will appear, not as a single edge/line, but instead as a concatenation of several much smaller lines randomly distributed along the true original edge/line, with slightly different coordinates. The application of the HT can in this case provide a more clear identification of the single coordinate of that edge/line around which the small fragments are detected by the edge detector, thus helping find a unique coordinate for each edge/line delimiting each SA. After the edge detection step, the HT is applied to extract the coordinates of the lines delimiting the SAs in a spectrogram.

The output of the HT will contain peaks at the coordinates that are more often observed and therefore the most likely candidates to be the true edges of the SA. These peaks can be extracted by setting an appropriate threshold. In this work, this threshold is set as a percentage of the maximum value of the HT (several thresholds will be tested in order to find the most convenient configuration). Following the extraction of the peaks in the HT, a clear indication of the coordinates of the lines in the spectrogram will be obtained. However, notice that these lines will only determine a grid of vertical and horizontal lines over the spectrogram but will not indicate in which of those rectangles in the grid a SA is actually contained. To resolve this problem, the pixel density in each rectangular region of the grid is calculated and if it is above a properly defined threshold then a SA will be assumed to be present. Notice that in those rectangles of the grid where a SA is actually present, the density of busy/occupied pixels will be higher than in those other rectangles placed within SAs, where no signal components should be present (except for some random false alarms). Following this procedure, it is possible to identify the rectangles where a SA is present and therefore extract the coordinates and dimensions of each SA in the spectrogram.

The proposed method is applied following two different approaches. The first approach attempts to isolate each SA component from the spectrogram before applying the procedure above. As a result, the procedure above will be applied individually to a set of subimages, each of which contains a single SA, which should presumably (but not necessarily) be located in the central rectangle of the subimage. The second approach applies the procedure above to the whole spectrogram, without attempting to isolate individual SA components. As a result, the procedure above will provide together the

coordinates of all the SAs found in the spectrogram. The complete set of steps for both approaches are detailed below.

Approach 1:

1) Filter input image to reduce incidence of false alarms.
2) Find connected components in the binary image in order to calculate the number of objects (blobs) in the image.
3) Trace region boundaries around each object/blob obtained above. These boundaries will divide the original image/spectrogram into a number of non-overlapping subimages/components. Each of such components will contain a single SA that will be processed individually repeating the steps below for each detected component.
4) In each component detected above:
   a) Find edges with a Canny edge detector.
   b) Apply the HT to the output of the edge detector.
   c) Identify the peaks of the HT by applying a threshold to the HT, which is calculated as a fraction/percentage of the maximum value of the HT.
   d) Identify *two* vertical lines and *two* horizontal lines. This assumes that a single SA will be present in the current component (assuming that region boundaries have been properly traced in Step 3).
   e) The four lines identified above will define a grid with 9 rectangular regions, where in principle only one of them should contain a SA. Such region can be identified by calculating the percentage of occupancy (i.e., percentage of busy pixels) and comparing to a properly set occupancy threshold.
   f) In the rectangular region where a SA is deemed to be present, extract its coordinates (for its delimiting vertical and horizontal lines) and add it to the final output image/spectrogram.

Approach 2:

1) Filter input image to reduce incidence of false alarms.
2) Find edges with a Canny edge detector.
3) Apply the HT to the output of the edge detector.
4) Identify the peaks of the HT by applying a threshold to the HT, which is calculated as a fraction/percentage of the maximum value of the HT.
5) Identify *all* vertical lines and *all* horizontal lines. This does not make any assumption on the number of SAs present since the complete spectrogram/image is being processed as a whole in this case.
6) The lines identified above will define a grid with an arbitrary number of rectangular regions, any of them can potentially contain a SA. Such regions containing a SA can be identified by calculating the percentage of occupancy (i.e., percentage of busy pixels) and comparing to a properly set occupancy threshold.
7) In the rectangular region where a SA is deemed to be present, extract its coordinates (for its delimiting vertical and horizontal lines) and add it to the final output image/spectrogram.

Both approaches are considered to determine whether the individual processing of each region of the spectrogram can provide any performance improvements over the whole processing of the complete spectrogram as a single image.

IV. Evaluation Methodology

The performance of the methods proposed in this work is evaluated by means of Monte Carlo simulations and hardware experiments. Simulations were performed following the same procedure used in [15], [18]. The simulation procedure utilises multiple random two-dimensional time-frequency binary data grids containing channelised SAs with fixed bandwidth and random durations. The binary spectrograms representing the original activity of the transmitter are corrupted by introducing both false alarms (resulting from noise) and missed detections (resulting from propagation impairments) with predefined probabilities. The corrupted spectrograms are then processed with the proposed SAE methods and the output is compared to the original spectrogram generated at the transmitter in order to assess the accuracy of the estimated SAs. The process is described in more detail in the steps below.

Step 1. *Create clean time-frequency test grids:* For each simulated SNR, a group of 100 test grids is randomly generated with resolution of 50×100 tiles, which can be considered of medium size according to [18]. The horizontal size (100 tiles) is the number of frequency bins while the vertical size (50 tiles) is given by the time resolution of the spectrum measurements. Busy/idle transmissions are randomly drawn from exponential distributions with rate parameters $\lambda_{on} = \lambda_{off} = 0.5\ s^{-1}$ and minimum busy/idle durations of $10\ s$ and $5\ s$, respectively. A total of three frequency channels with equal bandwidths are considered, however only the central one is used, and guard bands of 5% of the channel bandwidth are taken into account. The test grids generated in this step represent the original transmission pattern of the transmitter before the signal passes through the radio channel and is corrupted by internal/external noise/interference and radio propagation mechanisms. Fig. 4a shows an illustrative example of one single channel in the test grid.

Step 2. *Add errors to the test grids:* Errors are added to the clean test grids generated in Step 1, affecting both idle tiles (via false alarms) and busy tiles (via signal missed detections). Idle/busy tiles can randomly change to busy/idle state with probability of false alarm P_{fa} / probability of missed detection $1 - P_d$, respectively. These probabilities are calculated assuming that the samples of the power spectrogram are converted to binary idle/busy states using an ED technique with a constant false alarm rate $P_{fa} = 0.01$ and an SNR-dependent detection probability P_d [18, eqs. (1)-(2)]. The test grids generated in this step represent the pattern observed by the receiver after the target signals have propagated through the radio channel and have been degraded by propagation and internal/external noise/interference. Fig. 4b shows how the test grid of Fig. 4a is observed at the receiver after the application of ED with a decision threshold calculated for $P_{fa} = 0.01$ and a receiving SNR of –5 dB, for which $P_d \approx 0.49$.

Step 3. *Estimate the SAs:* This step involves the application of a SAE method to the (corrupted) noisy test grids obtained

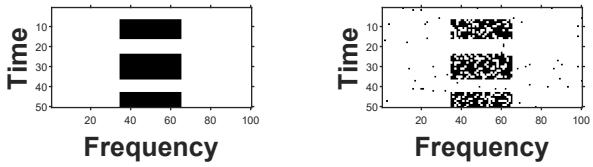

(a) (b)

Fig. 4: Example of a randomly generated time/frequency test grid: (a) Clean test grid, (b) Test grid with noise (SNR = –5 dB).

in Step 2 in order to estimate the SAs present in the clean test grid. In this step, the proposed SAE methods based on the HT are employed. The ED, CT-SA and SSA methods discussed in Section II-B are also simulated in this work in order to provide a point of reference to which the performance of the proposed methods is compared. The ED method has been selected as a basic reference, even though it cannot actually provide an estimation of the SAs present in an spectrogram. The CT-SA and SSA methods, which are specifically designed to detect SAs, have been selected for comparison because these methods can provide an automated estimation of the coordinates and dimensions of each SA and therefore provide a good reference for a fair comparison (as opposed to other SAE methods that are unable to provide this information in an automated manner). It is worth noting that the performance of the SSA method is sensitive to its configuration parameters. In this work, the SSA detection masks were adjusted according to [13, eqs. (3)–(4)], while the values for the sensitivity thresholds used by the algorithm were taken from [13]. This choice performs well but may not necessarily lead to a fine tuning of the SSA performance with the particular spectrum dataset employed in this study (an optimisation approach is discussed in [13], which is beyond the scope of this work).

Step 4. *Assess the accuracy of the estimated SAs:* This step involves the verification of the accuracy of the estimated SA obtained from Step 3. It is performed through a comparison between each original clean test grid generated in Step 1 and the corresponding test grid obtained in Step 3. The performance of SAE methods is assessed in this work in terms of the F1 score, which takes into consideration the possible imbalance between the number of tiles in idle and busy states in the original test grid. The F1 score is defined as [26]:

$$F1 = \frac{2 \times TP}{2 \times TP + FP + FN}, \tag{1}$$

where TP, FP and FN represent the number of true positive, false positive and false negative detections, respectively. The F1 score ranges within the interval $[0, 1]$, where the lower bound of the interval represents the worst detection performance and while the upper bound denotes perfect detection.

Simulation results were compared to experimental results obtained with the hardware prototype shown in Fig. 5, which was composed of a Signal Hound VSG25A vector signal generator as the signal transmitter, a short coaxial cable along with a 20 dB attenuator to emulate the transmission channel, and a Tektronix RSA306B real-time spectrum analyser as the signal receiver. A wired connection was employed to avoid unwanted interference to/from other wireless devices operating in the neighbourhood of the prototype. The transmitter and receiver were connected via USB to the same computer, where a Matlab control program was run to coordinate the operation of the transmitter and receiver and ensure that the data were correctly synchronised so they could be compared to assess the estimation accuracy. Such program was implemented using Matlab's Instrument Control Toolbox along with the libraries and Application Programming Interfaces (APIs) provided by the manufacturers.

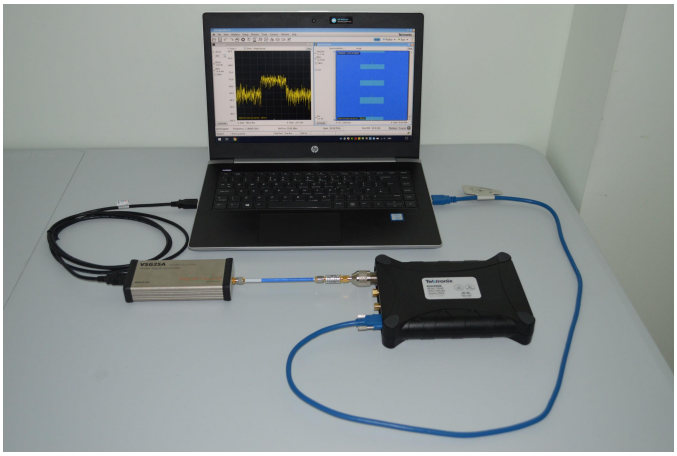

Fig. 5: Hardware prototype used in this work: vector signal generator (left), coaxial cable and attenuator, and spectrum analyser (right).

The experimental platform was configured to replicate the simulation configuration. The transmitted signal was a multi-tone signal with a spectral shape similar to an OFDM signal composed of 1001 unmodulated tones with random phase spaced at 10 kHz around a central frequency of 1 GHz, with a total signal bandwidth of 10 MHz. The centre frequency of the receiver was also configured to 1 GHz with a frequency span of 30 MHz (i.e., signal bandwidth was 1/3 of the frequency span). The relation between the transmission power configured at the signal generator and the SNR observed at the spectrum analyser was carefully calibrated to enable a fair comparison between simulation and experimental results.

V. Performance Evaluation

To illustrate the operation of the HT-based SAE methods proposed in this work, Figs. 6 and 7 show examples of the SA edges estimated by the proposed method based on Approaches 1 and 2, respectively. These figures represent the outcome of Step 4c for Approach 1 (aggregating the detections for each individual SA together in the same figure) and the outcome of Step 4 for Approach 2. The figures show for reference the edges detected by the Canny edge detector (Step 4a in Approach 1 and Step 2 in Approach 2) as thick white lines (notice that these SA edges are not perfectly rectangular due to the corruption produced by false alarms and missed detections). These figures also plot the detected peaks of the HT joined by straight lines for a more clear visualiation.

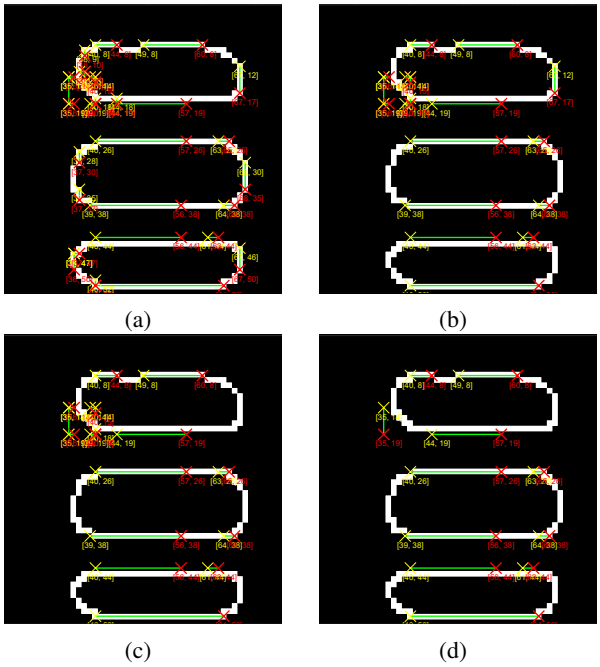

(a) (b) (c) (d)

Fig. 6: Examples of the SA edges estimated by the proposed HT method based on **Approach 1**. The peaks of the HT are identified based on the maximum value of the HT, $\max(\mathcal{H})$, using different thresholds equal to: (a) $0.1 \cdot \max(\mathcal{H})$, (b) $0.3 \cdot \max(\mathcal{H})$, (c) $0.5 \cdot \max(\mathcal{H})$, and (d) $0.7 \cdot \max(\mathcal{H})$ [SNR = –5 dB].

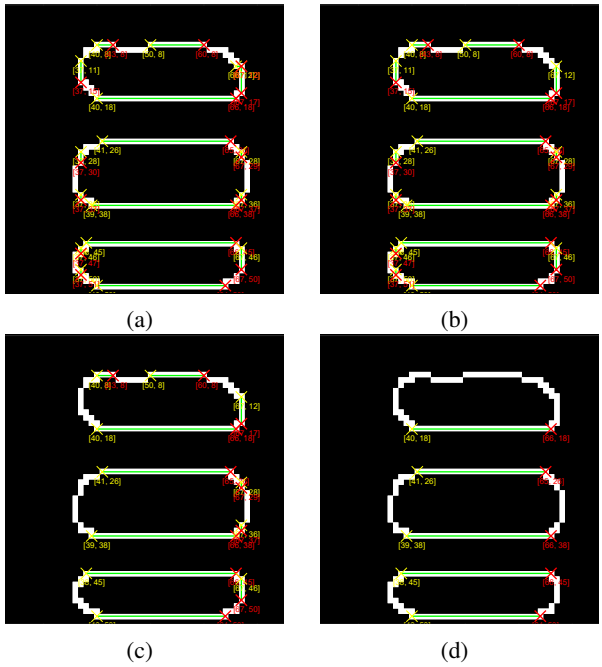

(a) (b) (c) (d)

Fig. 7: Examples of the SA edges estimated by the proposed HT method based on **Approach 2**. The peaks of the HT are identified based on the maximum value of the HT, $\max(\mathcal{H})$, using different thresholds equal to: (a) $0.1 \cdot \max(\mathcal{H})$, (b) $0.3 \cdot \max(\mathcal{H})$, (c) $0.5 \cdot \max(\mathcal{H})$, and (d) $0.7 \cdot \max(\mathcal{H})$ [SNR = –5 dB].

These peaks are identified based on the maximum value of the HT, denoted as $\max(\mathcal{H})$, using different thresholds equal to $0.1 \cdot \max(\mathcal{H})$, $0.3 \cdot \max(\mathcal{H})$, $0.5 \cdot \max(\mathcal{H})$ and $0.7 \cdot \max(\mathcal{H})$. By carefully inspecting these figures, one can notice that Approach 1 will only work with a threshold equal to $0.1 \cdot \max(\mathcal{H})$; selecting a threshold greater than this will lead to some of the edge components of the SAs being missed (in particular in some of the vertical edges). On the other hand, Approach 2 can detect relevant edges with thresholds equal to $0.1 \cdot \max(\mathcal{H})$ and $0.3 \cdot \max(\mathcal{H})$, however it will miss relevant edge components of the SAs if the threshold is set to $0.5 \cdot \max(\mathcal{H})$ or $0.7 \cdot \max(\mathcal{H})$. These results indicate that relevant peaks of the HT are observed at relatively low values and therefore the threshold to identify the peaks of the HT needs to be selected to an equally low value accordingly.

Another interesting observation that can be made from the comparison of Figs. 6 and 7 is that Approach 1 seems to misinterpret the edges of some small artefacts as edges of SA components. This can be clearly appreciated in the bottom-left corner of the top SA of Fig. 6, where a large number of lines/edges are detected. These are not edges of a genuine SA but simply the edges of small objects, possible fragments of the original SA or a relatively large number of false alarms that could not be removed in the false alarm removal step. Such small objects can potentially be classified as independent regions containing SAs in Step 3 of Approach 1 and each of them will be processed individually with the aim to detect a SA component in each of them, which leads to errors.

The observation above can be verified in Fig. 8, where it can be noticed that a small SA is attached to the bottom-left corner of the top SA detected in the final output of Approach 1. This seems to suggest that the principle of Approach 1, according to which each region in a spectrogram where a SA component is believed to be present is processed individually, may be counterproductive since certain artefacts may mislead the boundary tracing process of Step 3 and make it believe that there are potential SAs where none are actually present.

To confirm this observation, Figs. 9 and 10 show the equivalent result with Approach 2 for HT peak thresholds of $0.1 \cdot \max(\mathcal{H})$ and $0.3 \cdot \max(\mathcal{H})$ (which were observed above to provide good SA edge detection performance). In this case it can be observed that Approach 2 does not misinterpret small objects or artefacts in the input spectrogram as individual SAs due to its global processing of the whole spectrogram, which confirms the observation above regarding the limitations of Approach 1. However, it can be noticed in Figs. 9 and 10 that Approach 2 can detect SAs in some regions where no SAs are present. These erroneous regions seem to occur between regions where genuine SAs are present and the error may be due to some false alarms, which would be difficult to remove following the employed filtering process when they are present in small narrow gaps between SAs. However, as it can be seen in Figs. 9 and 10, this problem can be easily resolved by increasing the minimum percentage of busy tiles that are required in a region for it to be considered as a true SA. Configuring such threshold to 10% or 20% of the

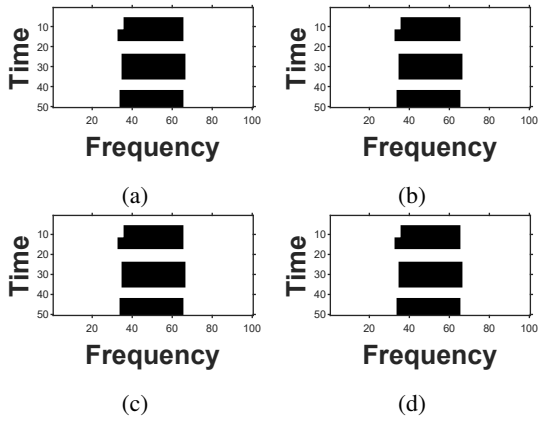

Fig. 8: Examples of the SAs estimated by the proposed HT method based on **Approach 1**. The peaks of the HT are identified based on the maximum value of the HT, $\max(\mathcal{H})$, using a threshold equal to $0.1 \cdot \max(\mathcal{H})$. The presence of SAs in the grid is detected with a percentage occupancy threshold of: (a) 10%, (b) 20%, (c) 30%, (d) Clean test grid (for reference) [SNR = –5 dB].

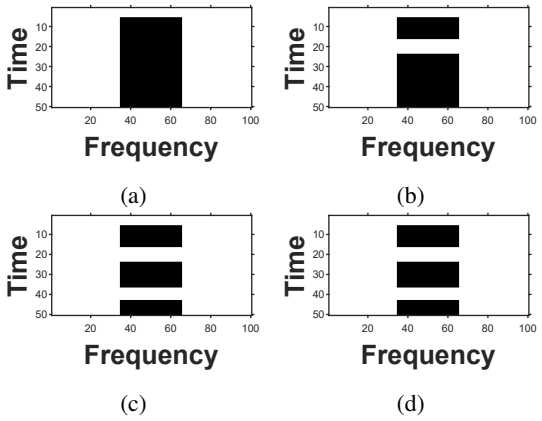

Fig. 9: Examples of the SAs estimated by the proposed HT method based on **Approach 2**. The peaks of the HT are identified based on the maximum value of the HT, $\max(\mathcal{H})$, using a threshold equal to $0.1 \cdot \max(\mathcal{H})$. The presence of SAs in the grid is detected with a percentage occupancy threshold of: (a) 10%, (b) 20%, (c) 30%, (d) Clean test grid (for reference) [SNR = –5 dB].

tiles in the rectangular region does not seem to be sufficient since the percentage of busy tiles present in those regions after applying the HT-based procedure is higher than these thresholds. However, increasing the value of the threshold to 30% is finally able to discriminate correctly between true SAs and regions containing small objects/artefacts. These results indicate that Approach 2 constitutes a preferred option compared to Approach 1 and that, with an adequate configuration of its parameters, Approach 2 can provide an accurate identification of the SAs present in a spectrogram.

Fig. 11 compares the performance of the proposed HT-based SAE method with that attained by the ED, CT-SA and SSA methods in terms of the F1 score, representing how accurately the detected SAs describe the original SAs generated by the transmitter. As it can be observed, Approach 2 provides a higher accuracy than Approach 1 at high SNR and slightly lower performance (with an almost negligible difference) at lower SNRs; these results also confirm that Approach 2 is a preferred option compared to Approach 1. When compared with the other SAE methods used as a reference, Approach 2 can achieve the best performance attained by the other methods in the region of higher SNR down to a minimum SNR of about –6 dB or –7 dB, which can be identified as the sensitivity of this SAE method. Above this SNR value, the accuracy obtained in terms of the F1 score is noticeably higher than that attained by the CT-SA and SSA methods and is only matched by the ED method. However, it is worth reminding that the ED method cannot extract automatically the coordinates and dimensions of the SA in the spectrogram and, in fact, it is unable to identify rectangularly shaped SAs. Only the CT-SA and SSA methods are able to do so, both of which provide an accuracy below that of the proposed HT-based method. This better accuracy obtained in the region of high SNR is obtained at the expense of a lower accuracy in the region of low SNR. However, it is worth noting that once

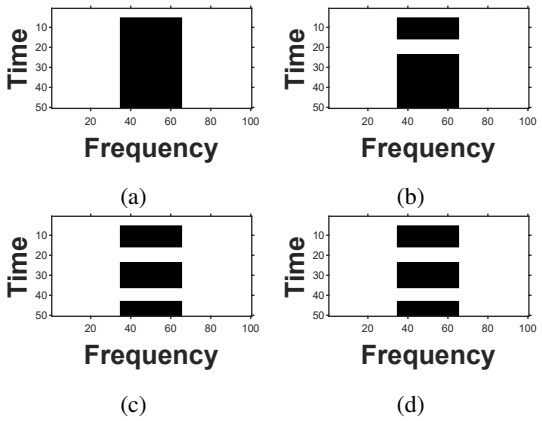

Fig. 10: Examples of the SAs estimated by the proposed HT method based on **Approach 2**. The peaks of the HT are identified based on the maximum value of the HT, $\max(\mathcal{H})$, using a threshold equal to $0.3 \cdot \max(\mathcal{H})$. The presence of SAs in the grid is detected with a percentage occupancy threshold of: (a) 10%, (b) 20%, (c) 30%, (d) Clean test grid (for reference) [SNR = –5 dB].

the F1 score decreases below a relatively high value (close to one) the detected SAs start to diverge noticeably from the original ones, both in numbers and dimensions. Therefore, a good detection accuracy in practical implementations requires an F1 score very close to one, around 0.9 and above, which can be obtained only under relatively high SNR conditions. Under such conditions, the proposed HT-based method can provide a more accurate detection of the SAs present in a radio spectrogram. It is also worth noting from Fig. 11 that the results obtained from software simulations provide a very close match with (and are therefore corroborated by) those obtained from hardware experiments.

Finally, Fig. 12 compares the computational costs of the different SAE methods considered in this work. As it can be observed, Approach 1 involves the highest computational

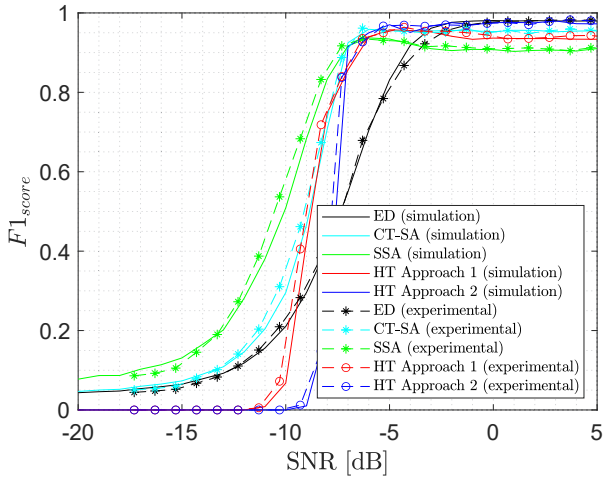

Fig. 11: F1 score as a function of the SNR for the different reference SAE methods (ED, CT-SA, SSA) and the proposed HT-based SAE method (Approaches 1 and 2, using in both cases the best configuration for each approach).

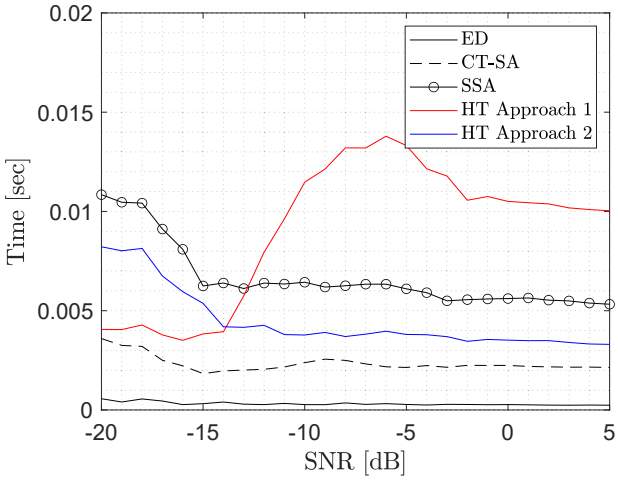

Fig. 12: Computational cost as a function of the SNR for the different reference SAE methods (ED, CT-SA, SSA) and the proposed HT-based SAE method (Approaches 1 and 2, using in both cases the best configuration for each approach).

load over most of the considered SNR interval due to its more complex procedure, which requires first isolating non-overlapping regions of the original spectrogram and then applying the proposed procedure to each region individually. This results in a significantly higher computational cost that, as seen in Fig. 11, cannot be justified based on the obtained accuracy performance. On the other hand, Approach 2 requires a significantly lower computational cost than Approach 1 in the SNR range of interest (i.e., higher SNR values), which can be explained by its more simple formulation where the whole spectrogram is processed as a single image; this not only reduces the computational burden of the proposed SAE method compared to Approach 1 but also, as seen in Fig. 11, provides more accurate results in the SNR range of interest. The computation time of Approach 2 is comparable to that of the reference methods. ED is the most lightweight method, as it could be expected, with CT-SA requiring a slightly higher computational cost (but lower than Approach 2) and SSA requiring a higher computational cost than the proposed method with Approach 2. Therefore, the proposed method (with Approach 2) not only can provide significantly accurate performance levels but can also do so at comparable costs than other existing SAE methods (and even lower in some cases).

VI. Conclusion

Radio communication signals are often represented in many practical application scenarios as a spectrogram, which indicates the power observed at several discrete time instants and frequency points within a certain time interval and frequency band, respectively. An accurate estimation of the Signal Area (SA) for each radio transmission contained in a spectrogram can provide valuable information in many practical application scenarios, such as autonomous spectrum-aware wireless communication systems. In this context, this work has proposed new methods for an accurate estimation based on the application of the Hough Transform (HT) combined with other techniques from the field of image processing. The performance of the proposed methods has been evaluated by means of simulations and the obtained results have shown that they can achieve a high level of SAE accuracy. An interesting feature of the proposed methods is their ability to extract automatically the coordinates and dimensions of each SA detected in a radio spectrogram. This feature can be useful in the automatic processing of radio spectrograms, for example in the context of autonomous spectrum-aware wireless systems.

References

[1] R. Mizuchi, K. Umebayashi, J. J. Lehtomäki, and M. López-Benítez, "A study on false alarm cancellation for spectrum usage measurements," in *Proc. IEEE Wireless Commun. and Networking Conf. (WCNC 2017), 3rd Int'l. Works. Smart Spectrum (IWSS 2017)*, Mar. 2017, pp. 1–6.

[2] T. Fujii and K. Umebayashi, "Smart spectrum for future wireless world," *IEICE Trans. on Comms.*, vol. 100, no. 9, pp. 1661–1673, Mar. 2017.

[3] Y. Chen and H.-S. Oh, "A survey of measurement-based spectrum occupancy modeling for cognitive radios," *IEEE Comms. Surveys & Tutorials*, vol. 18, no. 1, pp. 848–859, Oct. 2016.

[4] C. Hory, N. Martin, and A. Chehikian, "Spectrogram segmentation by means of statistical features for non-stationary signal interpretation," *IEEE Trans. Signal Process.*, vol. 50, no. 12, pp. 2915–2925, Dec. 2002.

[5] C. Smith, Q. R. Black, and M. Magee, "Computer vision for improved single-sensor spectrum sensing," in *Proc. Sensor Signal Processing for Defence (SSPD 2012)*, Sep. 2012.

[6] S. Phonsri, S. S. Mukherjee, and M. Sellathurai, "Computer vision and bi-directional neural network for extraction of communications signal from noisy spectrogram," in *Proc. IEEE Conf. Antenna Measurements and Applications (CAMA 2015)*, Dec. 2015, pp. 1–4.

[7] X. Zha, H. Peng, X. Qin, G. Li, and S. Yang, "A deep learning framework for signal detection and modulation classification," *Sensors*, vol. 19, no. 18, pp. 1–21, Sep. 2019.

[8] W. Liu, D. Anguelov, D. Erhan, C. Szegedy, S. Reed, C.-Y. Fu, and A. C. Berg, "SSD: single shot multibox detector," in *Proc. 14th European Conf. Computer Vision (ECCV 2016)*, Oct. 2016, pp. 21–37.

[9] W. Li, K. Wang, and L. You, "A deep convolutional network for multitype signal detection and classification in spectrogram," *Mathematical Problems in Engineering*, vol. 2020, pp. 1–16, Sep. 2020.

[10] Y. Zhou, Y. Feng, V. Tarokh, V. Gintautas, J. McClelland, and D. Garagic, "Multi-level mean-shift clustering for single-channel radio frequency signal separation," in *Proc. IEEE 29th Int'l. Works. Machine Learning for Signal Processing (MLSP 2019)*, Oct. 2019, pp. 1–6.

[11] J. Kokkoniemi and J. Lehtomäki, "Spectrum occupancy measurements and analysis methods on the 2.45 GHz ISM band," in *2012 7th international ICST conference on cognitive radio oriented wireless networks and communications (CROWNCOM)*. IEEE, Jun. 2012, pp. 285–290.

[12] K. Umebayashi, H. Iwata, J. J. Lehtomäki, and M. López-Benítez, "Study on simple signal area estimation for efficient spectrum measurements," in *Proc. 26th European Conf. Networks and Commun. (EuCNC 2017)*, Jun. 2017, pp. 1–5.

[13] K. Umebayashi, K. Moriwaki, R. Mizuchi, H. Iwata, S. Tiiro, J. J. Lehtomäki, M. López-Benítez, and Y. Suzuki, "Simple primary user signal area estimation for spectrum measurement," *IEICE Trans. Commun.*, vol. E99-B, no. 2, pp. 523–532, Feb. 2016.

[14] R. Mizuchi, K. Umebayashi, J. Lehtomäki, and M. López-Benítez, "A study on FFT-ED based signal area estimation for spectrum awareness," in *Proc. Int'l. Workshop on Smart Wireless Commun. (SmartCom 2016)*, IEICE Tech. Rep., vol. 116, no. 29, SR2016-9, pp. 27-34, May 2016.

[15] M. M. Alammar and M. López-Benítez, "A minesweeper algorithm for improved signal area estimation in spectrum aware systems," in *IEEE 28th International Conference on Telecommunications (ICT 2021)*, Jun. 2021, pp. 1–6.

[16] R. C. González and R. E. Woods, *Digital Image Processing*. Prentice Hall, 2002.

[17] H. Rohling, "Radar cfar thresholding in clutter and multiple target situations," *IEEE Transactions on Aerospace and Electronic Systems*, vol. AES-19, no. 4, pp. 608–621, 1983.

[18] M. M. Alammar and M. López-Benítez, "Evaluation of the impact of thresholding and frequency/time resolution on signal area estimation methods," in *IEEE 93rd Vehicular Technology Conference (VTC 2021-Spring), 7th IEEE International Workshop on Smart Spectrum (IWSS 2021)*, Apr. 2021, pp. 1–7.

[19] A. Krishnakumar and P. Krishnan, "On the accuracy of signal strength-based estimation techniques," in *Proceedings IEEE 24th Annual Joint Conference of the IEEE Computer and Communications Societies.*, vol. 1. IEEE, 2005, pp. 642–650.

[20] M. López-Benítez and J. Lehtomäki, "Energy detection based estimation of primary channel occupancy rate in cognitive radio," in *2016 IEEE Wireless Communications and Networking Conference Workshops (WCNCW)*, 2016, pp. 355–360.

[21] L. Cirillo, A. Zoubir, and M. Amin, "Parameter estimation for locally linear fm signals using a time-frequency hough transform," *IEEE Transactions on Signal Processing*, vol. 56, no. 9, pp. 4162–4175, 2008.

[22] N. Aggarwal and W. Karl, "Line detection in images through regularized hough transform," *IEEE Transactions on Image Processing*, vol. 15, no. 3, pp. 582–591, 2006.

[23] K. Zhao, Q. Han, C.-B. Zhang, J. Xu, and M.-M. Cheng, "Deep hough transform for semantic line detection," *IEEE Transactions on Pattern Analysis and Machine Intelligence*, pp. 1–1, 2021.

[24] J. Canny, "A computational approach to edge detection," *IEEE Transactions on Pattern Analysis and Machine Intelligence*, vol. PAMI-8, no. 6, pp. 679–698, Nov. 1986.

[25] B. Govindarajan, K. A. Panetta, and S. Agaian, "Image reconstruction for quality assessment of edge detectors," in *2008 IEEE International Conference on Systems, Man and Cybernetics*, 2008, pp. 691–696.

[26] D. Powers, "Evaluation: From precision, recall and F-measure to ROC, informedness, markedness and correlation," *J. Mach. Learn. Technol*, vol. 2, pp. 2229–3981, Jan. 2011.